High spin states of ^{37}Ar

Ananya Das,[1] Abhijit Bisoi,[1,*] M. Saha Sarkar,[2] S. Sarkar,[1] S. Ray,[3] D. Pramanik,[4] R. Kshetri,[5] S. Nag,[6] P. Singh,[7] K. Selvakumar,[8] A. Goswami,[2] S. Saha,[9] J. Sethi,[10] T. Trivedi,[11] B. S. Naidu,[9] R. Donthi,[9] V. Nanal,[9] and R. Palit[9]

[1]*Indian Institute of Engineering Science and Technology, Shibpur, Howrah 711103, India*
[2]*Saha Institute of Nuclear Physics, Bidhannagar, Kolkata 700064, India*
[3]*Mody University of Science and Technology, Sikar, Rajasthan 332311, India*
[4]*Haldia Institute of Technology, Haldia 721631, India*
[5]*Department of Physics, University of Burdwan, Burdwan 713104, India*
[6]*Department of Physics, Indian Institute of Technology (BHU), Varanasi 221005, India*
[7]*Ifru, CEA, Universite Paris-Saclay, F-91191 Gif-sur-Yvette, France*
[8]*Department of Physics, Bannari Amman Institute of Technology, Sathyamangalam 638401, India*
[9]*Tata Institute of Fundamental Research, Mumbai 400085, India*
[10]*Department of Chemistry and Biochemistry, University of Maryland, College Park, Maryland 20742, USA*
[11]*Department of Pure and Applied Physics, Guru Ghasidas Viswavidyalaya, Bilaspur 495009, India*

(Received 26 August 2019; revised manuscript received 25 November 2019; accepted 10 March 2020; published 20 April 2020)

High spin states of ^{37}Ar, populated through the ^{27}Al(^{12}C, np)^{37}Ar reaction with a 40 MeV ^{12}C beam, were studied using the Indian National Gamma Array (INGA) facility. The existing level scheme has been extended up to 10.5 MeV by adding some new levels and transitions. The spins and parities of the new levels were assigned from R_{DCO}, R_{ADO}, and linear polarization measurements. The spins and parities of the existing levels also were modified or confirmed in the present experiment. The multipole mixing ratios (δ) for most of the transitions were measured and compared with the earlier measurements wherever available. Large basis shell model calculations with different particle restrictions in sd and pf orbitals were performed to understand the microscopic origin of these levels. A simple two-level mixing calculation was also performed to extract the amount of multiparticle multihole configuration mixing for a few levels.

DOI: 10.1103/PhysRevC.101.044310

I. INTRODUCTION

Spectroscopic study of upper sd shell nuclei furnishes salient information about different interesting phenomena such as collective excitations, α clusters, etc. These nuclei generally exhibit single-particle type excitations, and large basis shell model (LBSM) calculations have successfully explained their excitation spectra [1]. Recent developments of detection systems made it possible to study these nuclei at higher angular momentum and excitation energy. As a result, apart from single-particle excitations, collective excitations have been observed at higher excitation energy in a few sd shell nuclei. The observation of superdeformed (SD) bands in even-even ^{36}Ar [2], ^{40}Ca [3], and odd-even ^{35}Cl [4] have generated new interest in this mass region. Shell model calculations with multiparticle multihole excitation have been carried out to understand the microscopic origin in these SD bands [4,5]. The presence of α-cluster structure of these SD bands has already been established [4,6,7]. Recently, the α-cluster structure was predicted in another non-α-conjugate nucleus, ^{34}S [8]. Therefore, this region gives us an opportunity to investigate the interplay between single-particle and collective modes of excitation both experimentally as well as theoretically using large basis shell model calculations.

^{37}Ar is an even-odd nucleus ($Z = 18$, $N = 19$). In our earlier studies, we investigated the high spin structure of two even-odd/odd-even nuclei, ^{33}S [9] and ^{35}Cl [4]. Both of these nuclei show collective excitations at higher excitation energies. In ^{35}Cl, a parity doublet SD band in the odd system has been reported for the first time in this mass region [4]. A candidate superdeformed band has also been identified in ^{33}S [9]. The neighboring isotopes of ^{37}Ar (^{36}Ar and ^{38}Ar) have also shown collective excitations at higher excitation energies. In ^{36}Ar, a positive parity SD band has been observed [2]. This band is generated from four-particle–four-hole (4p-4h) excitation [5]. Two normal deformed bands generated from 4p-4h excitation have also been reported in ^{38}Ar [10]. ^{37}Ar is one neutron away from ^{36}Ar (^{37}Ar $-1n$) and ^{38}Ar (^{37}Ar $+1n$). So, one may expect collective excitations generated from multiparticle multihole excitation at higher excitation energy in ^{37}Ar. Collective excitation has also been observed at higher excitation energy in ^{40}Ar [11]. So, a detailed spectroscopic study of ^{37}Ar at higher excitation energy is also very important to understand the evolution of collectivity in sd shell nuclei with increasing neutron number.

*Corresponding author: abhijitbisoi@physics.iiests.ac.in

^{37}Ar has been substantially investigated through proton-, deuteron-, and alpha-induced reactions [1]. However, only a few experimental data are available where heavy ion beams were used [1,12,13]. ^{37}Ar, populated through a heavy-ion induced reaction, was previously studied by Warburton *et al.* [14]. They extended the level scheme up to 7 MeV and assigned the spins and parities of most of the levels. In the present work, we have extended the level scheme of ^{37}Ar up to 10.5 MeV. The spectroscopic information of the excited levels and decay transitions have been measured and compared with the earlier measurements wherever available. LBSM calculations with different particle restrictions have been carried out to understand the microscopic origin of these levels.

In the following sections, we discuss in detail the experiment, data analysis techniques, experimental results, and theoretical investigations using LBSM calculations.

II. EXPERIMENTAL DETAILS AND DATA ANALYSIS

High spin states of ^{37}Ar were populated through the ^{27}Al(^{12}C, np)^{37}Ar fusion evaporation reaction at $E_{\rm lab}$ = 40 MeV. The ^{12}C beam was provided by the 14UD Pelletron accelerator at Tata Institute of Fundamental Research (TIFR), Mumbai. The target ^{27}Al (0.5 mg/cm^2) was prepared with ^{197}Au (10 mg/cm^2) backing to stop the recoils. A multi-detector array (INGA setup), comprising 15 Compton suppressed clovers, was used to detect the γ rays [15]. These fifteen detectors were mounted at six different angles, i.e., 157° (3), 140° (2), 115° (2), 90° (4), 65° (2), and 40° (2) with respect to the beam axis. About 6×10^8 twofold γ-γ coincidence events were recorded in list mode using a digital data acquisition system based on Pixie-16 modules, developed by XIA LLC [16]. The data sorting program, multiparameter timestamp-based coincidence search (MARCOS), developed at TIFR was used to generate angle-independent symmetric and angle-dependent asymmetric $E\gamma$-$E\gamma$ matrices, which were analyzed using INGASORT [17] and RADWARE [18] software. Singles data were collected in list mode for relative intensity and angular distribution measurements.

In this mass domain, most of the emitted γ rays from the excited states of the nuclei have energies $\geqslant$1000 keV. But, there is no easily available radioactive sources in a laboratory which emit γ rays higher than 1500 keV. Therefore, in the same setup, ^{66}Ga was produced through a fusion evaporation reaction, where a ^{13}C beam with energy 50 MeV was incident on ^{56}Fe. Energy and relative efficiency calibrations were therefore performed with ^{152}Eu, ^{133}Ba, and ^{66}Ga radioactive sources.

In order to build up the level scheme of ^{37}Ar, angle-independent and -dependent (90° vs 90°) symmetric γ-γ matrices were used. A total projection spectrum as well as typical gated spectra are shown in Fig. 1. The predicted relative cross section, using PACE4 [19], of the ^{27}Al(^{12}C, np)^{37}Ar channel was 17.8% of the total fusion. Therefore, the γ rays from nuclei populated through other dominant channels of the reaction are also marked in Fig. 1. The multipolarity of γ ray transition was determined from the directional correlation of γ rays emitted from excited oriented states (DCO) measurement. The DCO ratio of a γ transition is defined as the ratio of

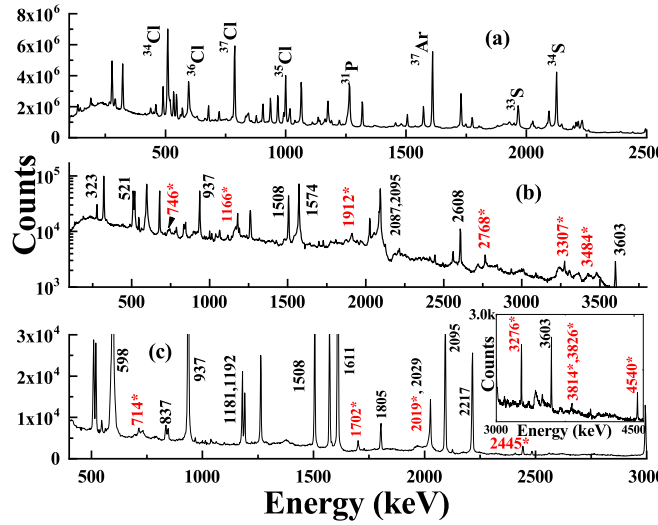

FIG. 1. (a) A total projection spectrum of γ rays emitted by different nuclei from the present experiment. Background subtracted coincidence spectra obtained by putting a gate on (b) 1611- and (c) 323-keV transitions. The spectrum of energies from 3 to 4.6 MeV, gated by the 323 keV transition, is shown in the inset of (c). The transition energies are shown in keV. Newly assigned transitions (red) are marked by asterisks.

intensities of that γ ray for two different angles in coincidence with another γ ray of known multipolarity. It is defined by

$$R_{\rm DCO} = \frac{I_{\gamma_1} \text{ observed at angle } \theta, \text{ gated by } \gamma_2 \text{ at } 90^\circ}{I_{\gamma_1} \text{ observed at angle } 90^\circ, \text{ gated by } \gamma_2 \text{ at } \theta}. \quad (1)$$

The $R_{\rm DCO}$ value depends on the multipolarities of these transitions, the angle between the detectors, and the amounts of mixing present in both the transitions. The experimental data were sorted into different angle-dependent asymmetric matrices for DCO measurement. In this analysis, the DCO ratios were determined for $\theta = 157^\circ$. The DCO ratio of each γ transition was obtained by putting a gate on a γ transition whose multipolarity and mixing ratio is known. For stretched transitions of the same multipolarity the DCO value is close to unity, and for a stretched dipole (quadrupole) transition gated by a pure quadrupole (dipole) it is nearly 0.5(2). For a mixed transition, it deviates from unity or 0.5(2). To assign the spin and extract the multipole mixing ratio (δ), the experimental DCO ratio was compared with the theoretical values using the computer code ANGCOR [20]. In this work, the spin alignment parameter $\sigma/J = 0.3$ [21] was used to determine the multipole mixing ratio (δ).

The DCO measurement could not be carried out for a few transitions due to their low statistics. So, we determined their multipolarities from the angular distribution from oriented nuclei (ADO) ratios. Two asymmetric matrices, having all the detectors (except the detectors used in the second axis) on first axis and the detectors at 90° and 157°, respectively, on the second axis, were constructed for ADO measurement. The ADO ratio ($R_{\rm ADO}$) of a transition is defined as the ratio of the intensities of that transition at two different angles (second axis) gated by other transition on the first axis. It is

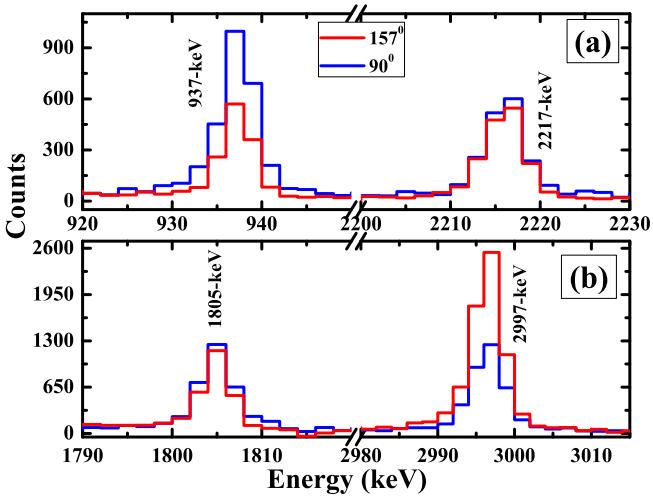

FIG. 2. A schematic representation of (a) DCO and (b) ADO spectra in ^{37}Ar. These spectra (a) and (b) are generated by putting gates on 2997 and 2217 keV, respectively.

expressed as

$$R_{\mathrm{ADO}} = \frac{I_{\gamma_1} \text{ measured at } 157^\circ, \text{ gated by } \gamma_2 \text{ at all}}{I_{\gamma_1} \text{ measured at } 90^\circ, \text{ gated by } \gamma_2 \text{ at all}}. \quad (2)$$

For the present setup, the $R_{\mathrm{ADO}} \approx 0.8$ for pure dipole transition and ≈ 1.7 for pure quadrupole transition. These values are estimated from the measured R_{ADO} values of a few known pure dipole and quadrupole transitions. In the case of mixed transitions, the ADO ratios deviate from those values under pure conditions and the values depend on the extent of mixing (δ). The ADO measurement was also carried out for a few strong transitions whose multipolarities were evaluated from the DCO measurement to confirm the assignment. A schematic representation of DCO and ADO spectra are shown in Fig. 2.

In order to assign the electric or magnetic nature of the transition, measurement was performed using integrated polarization directional correlation of oriented nuclei (IPDCO) [22]. For that purpose two asymmetric $E\gamma$-$E\gamma$ matrices, named parallel and perpendicular, were constructed. In the parallel (perpendicular) matrix, the simultaneous events fired in the two crystals of 90° clovers which are parallel (perpendicular) to the emission plane are recorded in the first axis and, on the second axis, the coincident γ rays fired in any other clovers are recorded. The polarization asymmetry then expressed as

$$\Delta_{\mathrm{IPDCO}} = \frac{a(E_\gamma)N_\perp - N_\parallel}{a(E_\gamma)N_\perp + N_\parallel} \quad (3)$$

where $N_\perp$ and $N_\parallel$ are the intensities of the full peaks observed in the perpendicular and parallel matrices, respectively. The asymmetry correction factor $[a(E_\gamma)]$ represents the geometrical asymmetry of the clovers placed at 90°. It is defined as

$$a(E_\gamma) = \frac{N_\parallel}{N_\perp}. \quad (4)$$

In the present work, ^{152}Eu and ^{66}Ga radioactive sources were used to extract the asymmetry correction factor $[a(E_\gamma)]$. For the determination of Δ_{IPDCO}, we put a gate on γ's on the second axis and measured the intensities of the coincident γ's from the projected parallel and perpendicular spectra. The positive value of Δ_{IPDCO} implies a pure electric transition whereas the negative value indicates pure magnetic transition. In the case of $\Delta J = 0$ transition, this scenario is reversed and the positive (negative) value of Δ_{IPDCO} indicates the magnetic (electric) nature of the transition. For a mixed transition, the value comes close to zero and the sign depends on the amount of mixing.

The theoretical Δ_{IPDCO} values were calculated for a few transitions in ^{37}Ar by using the relation

$$P(\theta) = \frac{\Delta_{\mathrm{IPDCO}}}{Q}, \quad (5)$$

where $P(\theta)$ is the degree of polarization and Q is the polarization sensitivity of the polarimeter. Q depends on the energy of the γ ray and geometry of the polarimeter [22]. The dependency can be expressed by the relation

$$Q(E_\gamma) = Q_o(E_\gamma)(CE_\gamma + D), \quad (6)$$

where $Q_0(E_\gamma)$ depends on the energy of the γ ray but not on the multipolarity of the γ ray.

The theoretical value of $P(90^\circ)$ for each of the transitions was calculated from the attenuated angular distribution coefficients [23]. For each transition, we used the spins and parities of the initial and final states and the spin alignment factor to find the attenuated angular distribution coefficients. The mixing ratios for the transitions were taken from the present work or the literature [1]. The energy dependency of Q for the present setup were taken from our earlier measurement [24]. Finally, we multiplied the calculated $P(90^\circ)$ by $Q(E_\gamma)$ to get the theoretical Δ_{IPDCO}. The calculation procedure of theoretical Δ_{IPDCO} is discussed in detail in Ref. [21]. In the present work, we calculated the theoretical Δ_{IPDCO} values only for the dipole transitions whose mixing ratios (δ) are known and compared them with their experimental values.

III. RESULTS AND DISCUSSION

Results from the preliminary analysis of the present data have already been reported in Refs. [25,26]. In this article, we report our detailed experimental and theoretical investigations on ^{37}Ar.

We have extended the existing level scheme up to 10.5 MeV based on the coincidence relationship, relative intensities, and R_{DCO}, R_{ADO}, and Δ_{IPDCO} values of the γ transitions (Fig. 3). We have added 18 new γ's and 8 new levels to the existing level scheme. The relative intensity of most of the transitions was determined from the 1611-keV gated spectrum generated from the angle-independent symmetric matrix. However, for a few transitions, viz., 1260 and 1264 keV, we could not separate them in the 1611-keV gated spectrum. To get the relative intensity of 1260-keV transition, we measured the intensities of 937- and 1260-keV transitions from the 1508-keV gated spectrum and then normalized them with the intensity of the 937-keV transition obtained from the

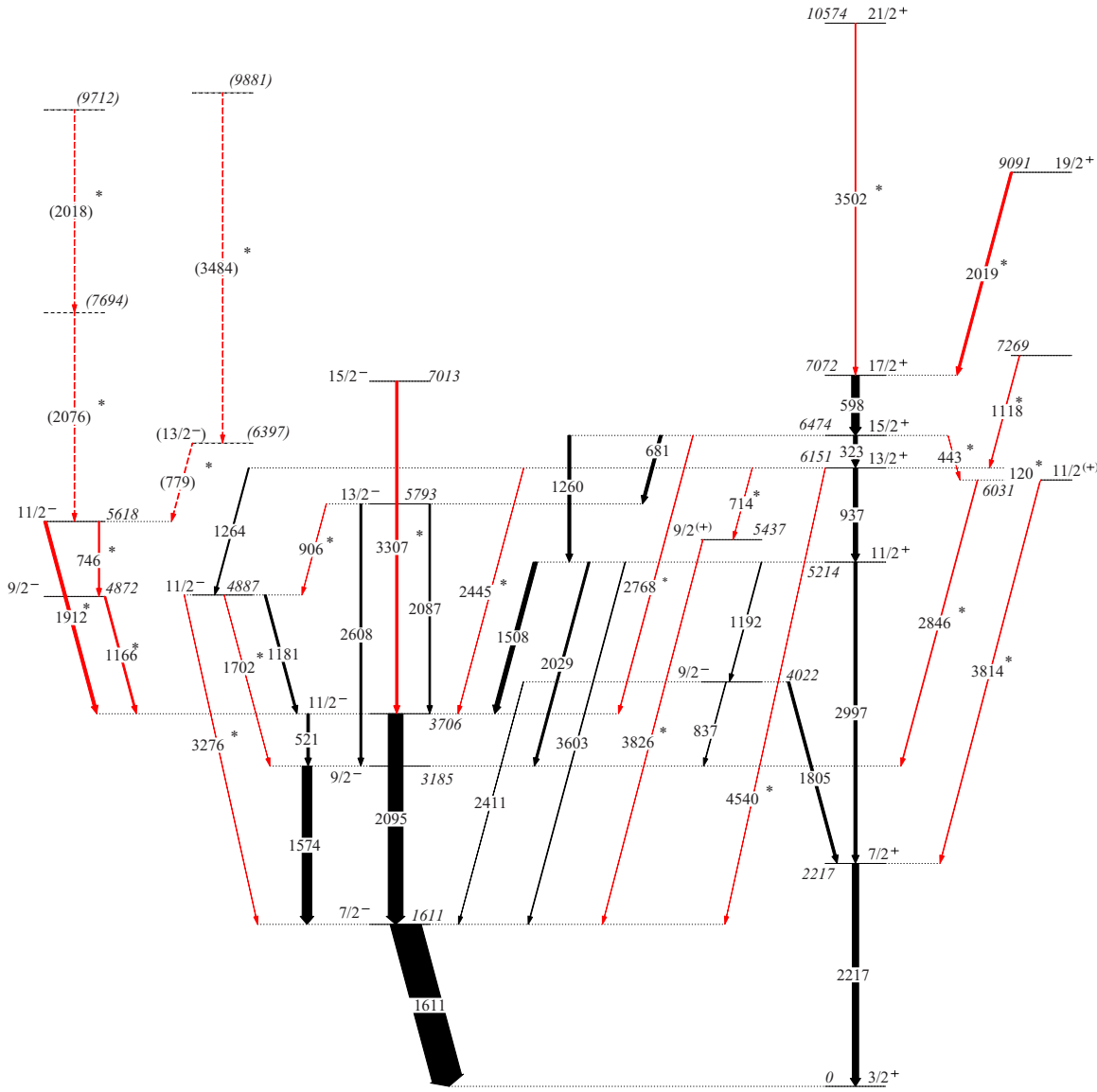

FIG. 3. Level scheme of ^{37}Ar. Energy levels are given in keV. Widths of the lines indicate their relative intensity. New γ transitions (red) are marked by asterisks. Tentative assignments are indicated by dashed lines.

1611-keV gated spectrum. Similarly, we measured the relative intensities of 1264-, 2019-, and 2029-keV transitions. During analysis, we found a few Doppler shifted peaks, viz., 598, 746, 779, 1166, 1574, 1912, 2019, 2095, 3307, 3484, 3502 keV, etc., in the 1611-keV gated spectrum, and a few of them are totally shifted. So, we used the 90° vs 90° symmetric matrix to measure the relative intensity of these transitions. The measured intensities of these Doppler shifted transitions were then normalized with the intensity of 1508-keV transition obtained in the 1611-keV gated spectrum generated from the angle-independent symmetric matrix. Using proper normalization, relative intensities of the 1611-keV transition and the transitions which are parallel to the 1611-keV transition were measured from the total projection spectrum. Finally, the relative intensities of all the transitions were normalized, considering the intensity of the 1611-keV transition to 100; they are listed in Table I.

The spins of the excited levels in ^{37}Ar were assigned or confirmed from $R_{\rm DCO}$ and $R_{\rm ADO}$ measurements. The multipole mixing ratios (δ) for a few mixed transitions were extracted from their measured $R_{\rm DCO}$ values and compared with the earlier measurements wherever available (Table I). We measured ten new multipole mixing ratios (δ) for the first time in ^{37}Ar. For a few transitions, viz., 837, 906, 1181, 1264 keV, etc., the $R_{\rm DCO}$ values were measured by putting a gate above the transition of interest and, due to the limitation of ANGCOR [20], we could not extract their multipole mixing ratios (δ). It was also noticed that multipole mixing ratios (δ) for a few $E2$ transitions were reported in the earlier measurements [14]. In the present work, based on our $R_{\rm DCO}$ and $R_{\rm ADO}$ measurements, we mention them as pure $E2$ transitions. The deviation of the $R_{\rm DCO}$ and $R_{\rm ADO}$ values of these transitions are due to the statistical fluctuation only. To assign or confirm the parity of the excited states, polarization measurement was carried out.

TABLE I. Relative intensity (I_{rel}), R_{DCO}, mixing ratio (δ), R_{ADO}, and Δ_{IPDCO} of the γ transitions in ^{37}Ar.

E_γ				E_{gate}			Mixing ratio (δ)			Δ_{IPDCO}	
(in keV)	I_{rel}	J_i	J_f	(in keV)	ΔJ	R_{DCO}	Present	Previous [14]	R_{ADO}	Expt.	Calc.
120(2)	0.16(3)	$13/2^+$	$11/2^{(+)}$								
323.0(6)	12.8(6)	$15/2^+$	$13/2^+$	1611	2	0.52(3)	0.08(3)	0.10(3)	0.79(4)	−0.07(1)	−0.09
443(2)	0.36(5)	$15/2^+$	$11/2^{(+)}$							0.05(4)	
521(1)	8.5(7)	$11/2^-$	$9/2^-$	1611	2	0.42(3)	0.02(2)	−0.03(10)	0.68(9)	−0.10(2)	−0.07
598.2(7)	25(2)	$17/2^+$	$15/2^+$	1611	2	0.46(3)	0.01(2)	0.03(3)	0.76(4)	−0.05(1)	−0.06
680.7(6)	9.8(5)	$15/2^+$	$13/2^-$	1611	2	0.46(3)	0.06(2)		0.86(4)	0.08(1)	0.05
714(2)	0.20(4)	$13/2^+$	$9/2^{(+)}$						1.40(27)		
746(2)	3.8(4)	$11/2^-$	$9/2^-$	1611	2	0.39(8)	−0.04(7)		0.57(12)	−0.08(3)	−0.06
779(2)	2.5(4)	$(13/2^-)$	$11/2^-$	1611	2	0.37(9)	$-0.07^{+0.09}_{-0.11}$		0.48(8)	−0.07(4)	−0.05
837(2)	1.5(3)	$9/2^-$	$9/2^-$	1192	1	2.16(20)			1.33(25)	0.03(1)	
906(2)	0.9(1)	$13/2^-$	$11/2^-$	681	1	1.02(27)			0.94(16)	−0.15(6)	
936.8(6)	14.4(7)	$13/2^+$	$11/2^+$	2217	2	0.64(4)	$0.15^{+0.02}_{-0.03}$	−0.14(3)	0.91(4)	−0.05(1)	−0.08
1166(1)	5.5(4)	$9/2^-$	$11/2^-$	1611	2	0.61(8)	−0.14(8)			−0.07(2)	−0.05
1181(1)	6.8(4)	$11/2^-$	$11/2^-$	323	1	2.06(48)			2.02(26)	0.04(2)	
1192(1)	2.3(2)	$11/2^+$	$9/2^-$	2217	2	0.61(8)	0.14(6)	−0.11(5)	0.81(9)	0.07(4)	0.07
1260(1)	9.8(8)	$15/2^+$	$11/2^+$	2217	2	0.92(16)	$E2$	0.04(3)	1.59(23)	0.05(2)	
1264(1)	3.5(3)	$13/2^+$	$11/2^-$	323	1	0.96(14)			0.91(11)	0.06(3)	
1507.6(8)	14.6(11)	$11/2^+$	$11/2^-$	1611	2	0.96(12)	$0.02^{+0.28}_{-0.20}$	0.09(6)	1.57(16)	−0.04(2)	
1573.8(8)	32(2)	$9/2^-$	$7/2^-$	1611	2	0.93(13)	$0.47^{+0.10}_{-0.09}$	−0.49(8)	1.56(13)	−0.09(1)	−0.11
1611.1(6)	100 (5)	$7/2^-$	$3/2^+$	937	1	1.88(17)	0.13(6)	0.14(5)	1.84(14)	−0.05(1)	
1702(2)	0.7(1)	$11/2^-$	$9/2^-$	1611	2	0.53(24)	$0.12^{+0.20}_{-0.27}$		0.74(26)		
1805(1)	8.3(13)	$9/2^-$	$7/2^+$	2217	2	0.52(8)	$0.09^{+0.06}_{-0.08}$		0.84(12)	0.08(2)	0.06
1912(2)	9.9(10)	$11/2^-$	$11/2^-$	1611	2	0.72(16)	$-0.38^{+0.30}_{-0.25}$		0.90(16)	0.05(2)	
2019(3)	7.4(8)	$19/2^+$	$17/2^+$	681	1	0.86(18)	$-0.01^{+0.09}_{-0.11}$		0.93(17)	−0.02(1)	−0.04
2029(1)	6.9(6)	$11/2^+$	$9/2^-$						0.95(17)	0.05(3)	
2087(2)	5.1(4)	$13/2^-$	$11/2^-$						1.12(19)	−0.14(4)	
2094.8(7)	49(4)	$11/2^-$	$9/2^-$	1508	0	1.07(10)	$E2$	0.02(3)	1.72(15)	0.03(1)	
2216.7(7)	21(4)	$7/2^+$	$3/2^+$	937	1	2.01(16)	$E2$	0.03(5)	1.68(11)	0.06(1)	
2411(2)	0.7(1)	$9/2^-$	$7/2^-$								
2445(2)	0.9(1)	$13/2^+$	$11/2^-$	1611	2	0.60(21)	$0.17^{+0.17}_{-0.19}$		1.15(25)	0.16(9)	
2608(2)	6.2(4)	$13/2^-$	$9/2^-$	1611	2	0.90(12)	$E2$	0.05(5)	1.76(12)	0.06(1)	
2768(2)	1.6(2)	$15/2^+$	$11/2^-$	1611	2	1.19(30)	$0.30^{+0.55}_{-0.36}$		2.03(40)	−0.10(6)	
2846(2)	2.3(3)	$11/2^{(+)}$	$9/2^-$						0.95(29)		
2997(1)	10.4(8)	$11/2^+$	$7/2^+$	2217	2	1.09(13)	$E2$	−0.08(8)	1.67(14)	0.04(3)	
3276(2)	1.1(1)	$11/2^-$	$7/2^-$	323	1	1.89(44)	$E2$		1.98(34)	0.04(2)	
3307(3)	7.3(6)	$15/2^-$	$11/2^-$	1611	2	0.92(14)	$E2$		1.49(16)	0.03(1)	
3502(3)	2.6(4)	$21/2^+$	$17/2^+$	323	1	2.04(33)	$E2$		1.70(20)	0.07(3)	
3603(2)	2.1(2)	$11/2^+$	$7/2^-$	1611	2	1.38(28)			2.64(35)	−0.11(5)	
3814(3)	1.8(3)	$11/2^{(+)}$	$7/2^+$						1.76(61)		
3826(4)	1.1(1)	$9/2^{(+)}$	$7/2^-$						0.49(18)		
4540(3)	0.7(1)	$13/2^+$	$7/2^-$	323	1	1.67(39)			3.34(58)	0.15(4)	

We measured the polarization asymmetry (Δ_{IPDCO}) for most of the transitions in ^{37}Ar and compared them with the calculated values (Table I). In Fig. 4, we have plotted the measured values of (a) R_{DCO} and (b) Δ_{IPDCO} for a few transitions in ^{37}Ar. The calculated Δ_{IPDCO} values are also shown in Fig. 4(b). The branching ratios of the excited states were measured from the present experimental data independently, i.e., the gate was put above the γ of interest and compared with the earlier measurements (Table II).

In order to extract the uncertainties in the measured intensities, we have considered both the statistical errors and the errors coming from the detector efficiencies. Similarly, we have taken care of both the fitting errors and the calibration errors to measure the uncertainties in the gamma energies. Uncertainties quoted in the measured values of intensities, R_{DCO}, R_{ADO}, and branching ratios (Table I and II) are therefore due to both statistical and detector efficiency. The uncertainties in the measured energies of the γ rays are due to the fitting and calibration errors. Since, we have used the same 90° detectors for $N_\perp$ and $N_\parallel$, the efficiency corrections of the 90° detectors are not considered in Δ_{IPDCO} measurements. Therefore, the uncertainties quoted in the measured values of Δ_{IPDCO} (Table I) are statistical only.

In the present work, a few new transitions like 2018-, 2076, and 3484 keV were observed at higher excitation energy. However, due to their low statistics, we could not measure

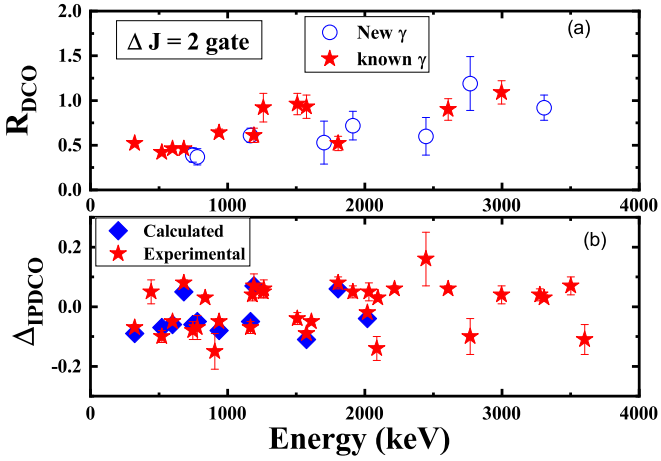

FIG. 4. (a) Experimental R_{DCO} values of a few transitions of ^{37}Ar. (b) Comparison of experimental and calculated polarization asymmetry (Δ_{IPDCO}) as a function of γ energy.

their spectroscopic properties and we placed them tentatively in the level scheme. In the following sections, we discuss our results in detail.

A. Levels with excitation energy ⩽6 MeV

At low excitation energy (⩽6 MeV), three new excited levels (4872, 5437, and 5618 keV) and seven new transitions (746, 906, 1166, 1702, 1912, 3276, and 3826 keV) have been added to the existing level scheme of ^{37}Ar. The spin and parity of the 5618-keV level were assigned based on the measured R_{DCO}, R_{ADO}, and Δ_{IPDCO} values of the decay out 1912-keV transition. The measured R_{DCO} value of the 1912-keV transition is 0.72(16) and has positive Δ_{IPDCO}, as shown in Table I. From ANGCOR [20], it was found that the calculated R_{DCO} of 1912 keV is 0.42 as a pure dipole ($\Delta J = 1$) transition and 0.90 as a pure quadrupole ($\Delta J = 2$) transition. Therefore, 1912 keV is either an electric dipole transition with $\delta \approx 0.27(8)$ or an electric quadrupole transition with $\delta \approx -0.2(1)$. In the case of the $\Delta J = 0$ transition, positive (negative) Δ_{IPDCO} value represents the magnetic (electric) nature of the transition. So, 1912 keV may be a magnetic dipole transition with $\delta = -0.38^{+0.30}_{-0.25}$. Mostly, the $E1$ and $E2$ transitions are pure in nature. So we have ruled out these possibilities and assigned the 1912-keV transition as a magnetic dipole transition. Therefore, the assigned spin and parity of the 5618-keV level is $11/2^-$. The R_{DCO} of 746 keV gated by 1611 keV is 0.39(8) and the Δ_{IPDCO} value is negative. So, the 746-keV transition is a magnetic dipole transition and it is decaying from the 5618-keV ($11/2^-$) level. Hence, we have assigned the spin and parity of the level at 4872 keV as $9/2^-$. The measured R_{DCO} and Δ_{IPDCO} of the decay out 1166-keV transition (Table I and Fig. 3) also supports this assignment. The spin of the 5437-keV level was assigned based on the R_{ADO} values of 714- and 3826-keV transitions. The measured R_{ADO} values of 714- and 3826-keV γ's are 1.40(27) and 0.49(18) (Table I), confirming their quadrupole and dipole natures, respectively. We could not measure the R_{DCO} and Δ_{IPDCO} of these transitions due to their low statistics. Therefore, we have assigned only the spin of the 5437-keV level as 9/2.

Previously, the spin of 4887-keV level was assigned as ⩾9/2 [14]. In the present work, we have removed this uncertainty based on the measured R_{DCO} and Δ_{IPDCO} values of the 1181-, 1264-, and 3276-keV transitions (Table I). Our result shows that 1181 keV is a magnetic dipole transition, 1264 keV is an electric dipole transition, and 3276 keV is an electric quadrupole transition. Therefore, we have assigned

TABLE II. Comparison between experimental and theoretical branching ratios of different excited levels.

		Branching ratio		
E_x	E_γ	Expt.		Theory
(keV)	(keV)	Present	Previous [14]	
1611	1611	100	100	
2217	2217	100	100	
3185	1574	100	100	
3706	521	16(3)	18(2)	18.8
	2095	84(3)	82(2)	81.2
4022	837	17.8(8)	36(4)	10.0
	1805	76(4)	58(6)	77.6
	2411	6.2(3)	6(2)	12.4
4872	1166	100		
4887	1181	71(3)	100	73.7
	1702	12(2)		7.6
	3276	17(2)		18.7
5214	1192	10.4(5)	12(3)	
	1508	38.4(20)	41(4)	
	2029	18.2(8)	16(4)	
	2997	27.5(10)	25(4)	
	3603	5.5(3)	6(3)	
5437	3826	100		
5618	746	25(5)		1.0
	1912	75(5)		99.0
5793	906	3.0(2)		6.0
	2087	39(2)	60(10)	35.0
	2608	58(2)	40(10)	59.0
6031	2846	56(4)		
	3814	44(4)		
6151	120	0.8(1)		
	714	1.8(1)		
	937	74(2)	75(5)	
	1264	18(1)	25(5)	
	2445	3.0(2)		
	4540	2.4(2)		
6397	779	100		
6474	323	45(1)	67(5)	
	443	1.4(1)		
	681	25(1)	28(5)	
	1260	26(1)	5(2)	
	2768	2.6(2)		
7013	3307	100		
7072	598	100		
7269	1118	100		
9091	2019	100		
10574	3502	100		

$11/2^-$ as the spin and parity of 4887-keV level. Due to the low statistics, we could only confirm the dipole nature of the 1702-keV transition.

The spins and parities of all other levels with excitation energy $\leqslant$6 MeV were confirmed in the present work. In this energy domain, we extracted the multipole mixing (δ) ratios for ten transitions and compared them with the earlier measurements if available. Most of the measured multipole mixing (δ) ratios agreed with the earlier measurements. In a few cases, viz., 1192- and 1574-keV transitions, the sign of mixing (δ) was changed. The previous authors measured the mixing ratios from a simultaneous consideration of the angular distribution and linear polarization results. But they did not mentioned the sign convention of the multipole mixing ratio (δ) explicitly. Their results are consistent with those obtained by Gadeken *et al.* [27]. Gadeken *et al.* [27] took the sign convention of the multipole mixing ratio (δ) from Ref. [28]. In the present work, we used the sign convention of the multipole mixing ratio (δ) as proposed by Krane and Steffen [29]. In their article [29], they used a consistent definition of the reduced matrix elements and compared them with the reduced multipole matrix elements of Rose and Brink [28]. It was mentioned in Ref. [29] that the reduced matrix elements are related to those of Rose and Brink [28] by a phase factor $(-1)^{I_i-I_f+L}$. I_i and I_f are the initial and final spin of the levels and L is the multipolarity of the transition. The sign of the mixing ratio obtained from these two conventions is therefore opposite, which is consistent with our present measurements.

In the present work, we also calculated the theoretical $R_{\rm DCO}$ of 1192- and 1574-keV transitions with their reported mixing ratios and compared them with the experimental values. For $\delta = -0.49$, the calculated $R_{\rm DCO}$ of 1574-keV transition is 0.14, whereas the experimental value is 0.93(13) (Table I). Similarly, in the case of the 1192-keV transition, the experimental $R_{\rm DCO}$ value is 0.61(8) (Table I) but the calculated $R_{\rm DCO}$ with $\delta = -0.11$ is 0.31. In both cases, the calculated $R_{\rm DCO}$ values deviated largely from the experimental values. So, we have reported the new mixing ratios of these transitions in Table I.

B. Levels with excitation energy between 6 and 9 MeV

In this energy domain, three new levels (6031, 7013, and 7269 keV) and nine new transitions have been added to the existing level scheme. In order to assign the spin and parity of the 6031-keV level, the spectroscopic properties of 120-, 443-, 2846-, and 3814-keV transitions were studied. These transitions are very weak in nature. So, we could only measure the $R_{\rm ADO}$ of 2846- and 3814-keV transitions. The measured $R_{\rm ADO}$ values of 2846- and 3814-keV transitions are 0.95(29) and 1.76(61), respectively. Based on these measured values, we assigned the spin of the 6031-keV level as 11/2. In order to assign the spin and parity of the 7013-keV level, the DCO and polarization measurements were carried out for the decay out 3307-keV transition. The measured $R_{\rm DCO}$, $R_{\rm ADO}$, and $\Delta_{\rm IPDCO}$ values of the 3307-keV transition are 0.92(14), 1.49(16), and 0.03(1), respectively (as shown in Table I) which confirm the electric quadrupole nature of the 3307-keV transition.

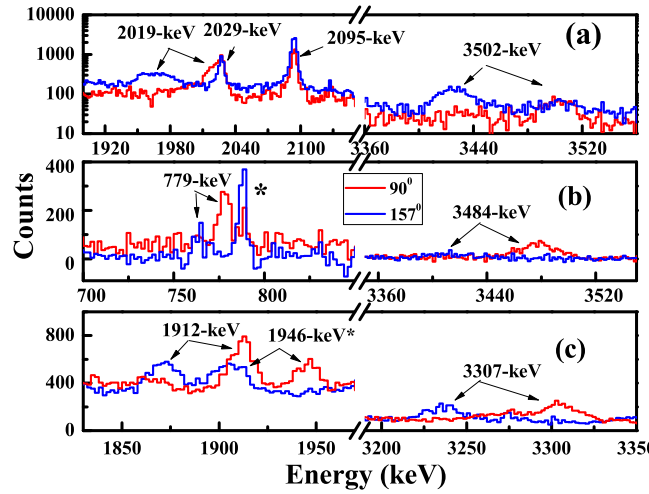

FIG. 5. Background subtracted coincidence spectrum obtained by putting a gates on (a) 323-, (b) 1912-, and (c) 1611-keV transitions. An angle dependent asymmetric matrix (157° vs 90°) was used to generate this spectrum. The shifted and unshifted position of these transitions at 157° and 90° are marked by the arrows. Transitions marked with an asterisk are the transitions from contaminants.

Therefore, the spin and parity of 7013-keV level were assigned as $15/2^-$. In this work, we could not assign the spin and parity of the 7269-keV level due to the very low statistics of the decay out 1118-keV transition.

The spin and parity of other levels in this energy domain were confirmed from DCO, ADO, and polarization measurements. The multipole mixing ratios (δ) for a few transitions were measured and compared with the previously reported values wherever available. In a few cases like 521- and 937-keV transitions, the sign of the multipole mixing ratio (δ) was changed. We have already discussed above the reason for these. Similarly to the 1192- and 1574-keV transitions, we also calculated $R_{\rm DCO}$ values of 521- and 937-keV transitions with the reported [14] mixings of 0.50 and 0.31, respectively. The calculated $R_{\rm DCO}$ values are far away from their measured values (Table I).

C. Levels with excitation energy >9 MeV

At higher excitation energy (>9 MeV), two new levels (9091 and 10574 keV) have been included in the existing level scheme. The decay out γ transitions (2019 and 3502 keV) from these levels are totally shifted as shown in Fig. 5(a). So, a 90° vs 90° symmetric matrix was used to place them in the level scheme. Our analysis shows that both 2019- and 3502-keV transitions are in coincidence with 598-, 323-, 937-, 2997-, and 2217-keV transitions. But they are not in coincidence with each other. So, we have placed them above the 598-keV transition as shown in Fig. 3. The spin and parity of these levels were assigned based on the $R_{\rm DCO}$, $R_{\rm ADO}$, and $\Delta_{\rm IPDCO}$ values of 2019-keV and 3502-keV transitions (Table I). As these transitions are comparatively weaker than other low-lying transitions, we have large errors in their measured $R_{\rm DCO}$, $R_{\rm ADO}$, and $\Delta_{\rm IPDCO}$ values.

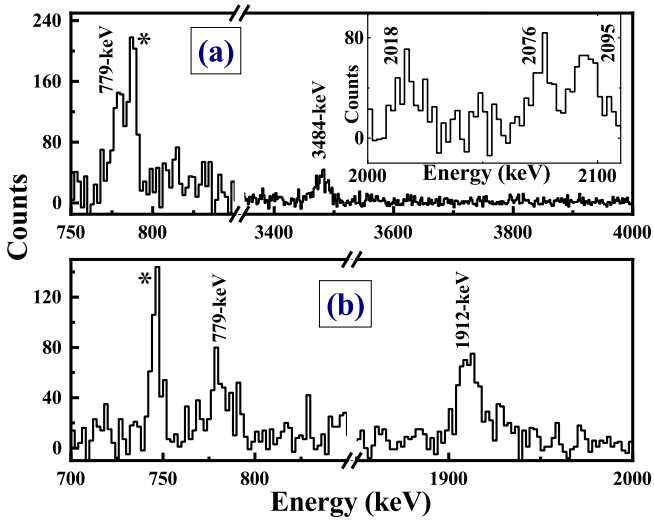

FIG. 6. Background subtracted coincidence spectra obtained by putting gates on (a) 1912- and (b) 3484-keV transitions. A 90° vs 90° symmetric matrix was used to generate these spectra. The presence of 2018- and 2076-keV transitions in the 1912-keV gated spectrum is also shown [(a), inset]. Transitions marked with an asterisk are the transitions from contaminants.

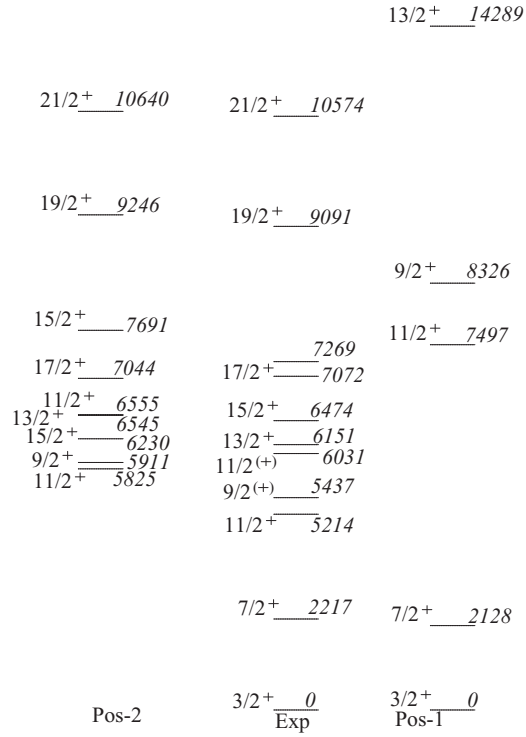

FIG. 7. Comparison of theoretical and experimental level schemes for positive parity states in ^{37}Ar. All these energies are plotted considering the ground state energy (−239.195 MeV) as 0.

In the present work, four new transitions (779, 2018, 2076, and 3484 keV) were observed in the 1912-keV gated spectrum [Fig. 6(a)]. These are very weak transitions and have large Doppler broadening. Among these four transitions, 779- and 3484-keV transitions are in coincidence with each other [Fig. 6(b)]. In order to place them in the level scheme, one has to measure their relative intensities, $R_{\rm DCO}$, $R_{\rm ADO}$, and $\Delta_{\rm IPDCO}$. Due to the low statistics and large Doppler broadening of 3484-keV transition, these measurements are only performed for the 779-keV transition. We have therefore placed them tentatively in the level scheme. The spin and parity of the 6397-keV level were assigned based on its present placement and the $R_{\rm DCO}$, $R_{\rm ADO}$, and $\Delta_{\rm IPDCO}$ values of the 779-keV transition. We could not establish the coincidence relationship between the other two transitions, i.e., 2018 and 2076 keV due to their low statistics. So we have placed them tentatively above the 1912-keV transition.

IV. THEORETICAL CALCULATION

In order to understand the microscopic origin of each of the excited states in ^{37}Ar, large basis shell model (LBSM) calculations were performed using the code OXBASH [30]. The valence space consists of $1d_{5/2}$, $1d_{3/2}$, $2s_{1/2}$, $1f_{7/2}$, $1f_{5/2}$, $2p_{3/2}$, and $2p_{1/2}$ orbitals for both neutrons and protons above the ^{16}O inert core. The number of valence particles (protons + neutrons) in ^{37}Ar is 21. The *SDPFMW* interaction [31] (as referred to within the OXBASH code package) was used for the calculation. The relevant details of this interaction are discussed in [31,32].

For nuclei having such a large number of valence particles in this large valence space, unrestricted calculations using the full model space are not always possible for all the excited states. Therefore, several particle restrictions in the model space were used during the calculation to reproduce the experimental energies. In the present work, we calculated the level energies and transition probabilities for most of the levels and transitions in ^{37}Ar. Different truncation schemes were adopted to reproduce these levels. Calculations with different truncations also indicate the minimum number of nucleons required in the pf shell to reproduce the high spin states. For all these calculations, the mass normalization constant, which was defined as the number of particles up to the *sd* shell, was considered accordingly. The details of these calculations are discussed in the next sections.

A. Positive parity states

We used two different truncations (Pos-1 and Pos-2) to reproduce the positive parity states in ^{37}Ar.

1. Pos-1

Calculation with 0p-0h excitation was carried out for the positive parity states in ^{37}Ar (Pos-1). In this calculation, all the valence particles are excited within the *sd* shell and 37 is the mass normalization factor. The maximum angular momentum that can be generated in this particle restriction is $13/2^+$. The calculated binding energy of ^{37}Ar (−239.195 MeV) is in good agreement with the experimental binding energy −239.197 MeV. It also reproduced the excitation energy of the $7/2^+$ level. However, the calculated energies for $J > 7/2^+$ are overpredicted by several MeV, as shown in Fig. 7. So we need

to consider the contribution from the neighboring pf shell for these positive parity excited states.

2. Pos-2

The calculation with 2p-2h excitation (Pos-2) was performed for the high spin positive parity states in ^{37}Ar. In this restriction, two particles are excited from the sd shell to the pf shell to reproduce the high spin positive parity states. The calculation was carried out with the full sd-pf model space and there is no particle restriction in the $1d_{5/2}$ orbital. The mass normalization factor for this calculation is 35. In Fig. 7, we have compared our calculated energies with the experimental values. It shows that the high spin positive parity yrast states ($15/2^+$, $17/2^+$, $19/2^+$, and $21/2^+$) are well reproduced (within 250 keV) with this particle restriction. However, the low-lying yrast $9/2^+$, $11/2^+$, and $13/2^+$ states are overpredicted by 400–600 keV. Apart from that, the sequence of $13/2^+$ and $15/2^+$ has been changed. Therefore, we need to consider the contributions from different particle excitations in the pf shell to improve their calculated energies. Note that the states $9/2^+$, $11/2^+$, and $13/2^+$ can be formed in 0p-0h excitation. Therefore, the overprediction in the calculated energies of these states is probably due to the missing of admixture of the 2p-2h and 0p-0h configurations. Admixture of 4p-4h configuration is also possible for these states. The *SDPFMW* interaction that was used in the calculations was developed for pure np-nh excitation. Therefore, it is not possible to perform a mixed calculation for these states.

B. Negative parity states

We considered 1p-1h excitation (Neg-1), i.e., only one nucleon is allowed into the pf shell to reproduce the negative parity states in ^{37}Ar. In this calculation, we use the full sd-pf model space and there is no particle restriction in the $1d_{5/2}$ orbital. The mass normalization factor for the sd shell two-body matrix elements (TBME) for this calculation is taken as 36. The result (Fig. 8) shows that the calculated energies of all the yrast negative parity states are underpredicted. The differences between the experimental and calculated energies (Δ_{Shell}) are $\approx$400 keV for the yrast $7/2^-$ and $9/2^-$ states and they decrease with the angular momentum and excitation energy. In order to improve the calculated energies of the negative parity states, one can change the effective single-particle energy of each of the pf orbitals by an amount of +300 keV. Since the high spin positive parity states ($\geqslant 15/2^+$) are well reproduced in 2p-2h excitation (Pos-2), we have not changed the single particle energies of the pf orbitals for the negative parity states.

It was also found that the calculated energies of $9/2^-_2$ and $9/2^-_3$ states are overpredicted. Interestingly, the excitation energy of $9/2^-_3$ (4872-keV) matches very well with the calculated energy of $9/2^-_2$. Therefore, both the 4022- and 4872-keV states are either mixed states (1p-1h + 3p-3h configuration) or the 4872-keV state is generated from pure 1p-1h excitation and only the 4022-keV ($9/2^-_2$) state is a mixed state. Due to computational limitations, the LBSM calculation using the full sd-pf model space is not possible for 3p-3h excitation in ^{37}Ar. Therefore, we could not confirm the microscopic origin of 4022- and 4872-keV states. We can only compare 4022- and 4872-keV states with the calculated $9/2^-_2$ and $9/2^-_3$ states, respectively, according to their sequence of occurrence.

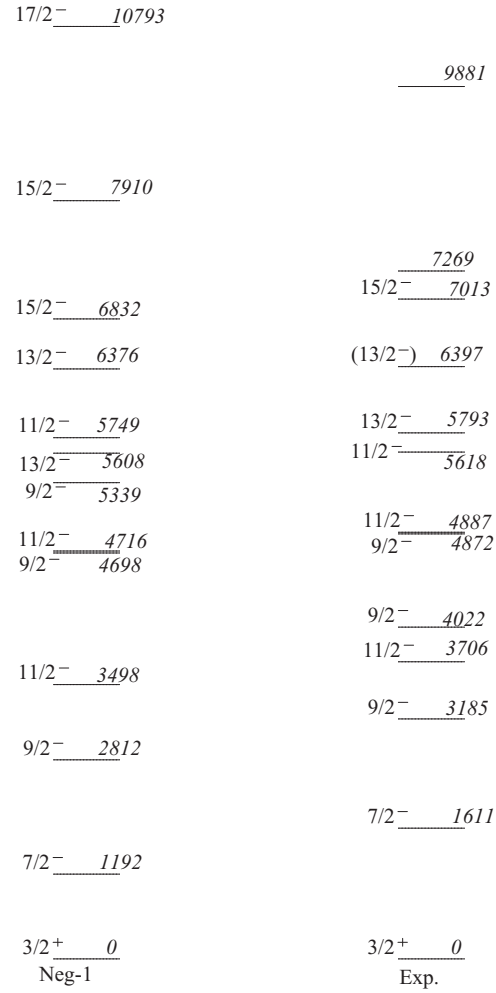

FIG. 8. Comparison of theoretical and experimental level schemes for negative parity states in ^{37}Ar. All these energies are plotted with respect to the ground state energy (−239.195 MeV) as 0.

C. Configuration mixing and collectivity

The decompositions of the wave functions for the positive and negative parity states in ^{37}Ar are shown in Tables III and IV, respectively. For the ground state ($3/2^+$) and the first excited positive parity state ($7/2^+$), we used the results obtained from 0p-0h excitation. Since the mixed calculation is not possible, results obtained from 1p-1h and 2p-2h excitations were considered for the remaining negative and positive parity states, respectively. The full sd-pf model space was used in these calculations.

A general particle partition is given by $(j_1^{m_1} \otimes j_2^{m_2} \otimes \cdots \otimes j_n^{m_n})$, where $m_1 + m_2 + \cdots + m_n = m$, m being the total number of valence particles. Due to the various intermediate couplings of angular momenta and isospins, a particle partition has many different configurations. The probability and the

TABLE III. Structure of the wave functions for the positive parity states in ^{37}Ar. The partitions are given in terms of occupation numbers of single-particle valence states in the following order: $1d_{5/2}$, $1d_{3/2}$, $2s_{1/2}$, $1f_{7/2}$, $1f_{5/2}$, $2p_{3/2}$, and $2p_{1/2}$. Those with $>10\%$ contribution in the wave function are shown in the table. N_1 is the total number of particle partitions, each of which contributes $>1\%$. N_2 gives the minimum number of particle partitions, each of which contributes $\leqslant 1\%$.

		Energy (MeV)		Wave function			
J_i^π	T	Expt.	Theor.	%	Partition	N_1	N_2
$3/2_1^+$	1/2	−239.197 0	(−239.195)	84	[12,5,4,0,0,0,0]	5	2
$7/2_1^+$	1/2	2.217	2.128	83	[12,5,4,0,0,0,0]	5	1
$11/2_1^+$	1/2	5.214	5.825	31	[12,3,4,2,0,0,0]	17	13
$9/2_1^+$	1/2	5.437	5.911	24	[12,3,4,2,0,0,0]	14	12
				16	[12,4,3,2,0,0,0]		
$11/2_2^+$	1/2	6.031	6.555	29	[12,3,4,2,0,0,0]	13	13
				13	[12,4,3,2,0,0,0]		
$13/2_1^+$	1/2	6.151	6.545	19	[12,4,3,2,0,0,0]	17	15
				17	[12,3,4,1,0,1,0]		
$15/2_1^+$	1/2	6.474	6.230	35	[12,3,4,2,0,0,0]	12	11
				11	[10,5,4,2,0,0,0]		
				10	[12,5,2,2,0,0,0]		
$17/2_1^+$	1/2	7.072	7.044	43	[12,3,4,2,0,0,0]	11	6
				12	[10,5,4,2,0,0,0]		
$19/2_1^+$	1/2	9.091	9.246	29	[12,4,3,2,0,0,0]	13	6
				14	[12,3,4,2,0,0,0]		
				14	[11,5,3,2,0,0,0]		
$21/2_1^+$	1/2	10.574	10.640	49	[12,3,4,2,0,0,0]	10	5
				14	[11,4,4,2,0,0,0]		

TABLE IV. Structure of the wave functions for the negative parity states in ^{37}Ar. The partitions are given in terms of occupation numbers of single-particle valence states in the following order: $1d_{5/2}$, $1d_{3/2}$, $2s_{1/2}$, $1f_{7/2}$, $1f_{5/2}$, $2p_{3/2}$, and $2p_{1/2}$. Those with $>10\%$ contribution in the wave function are shown in the table. N_1 is the total number of particle partitions, each of which contributes $>1\%$. N_2 gives the minimum number of particle partitions, each of which contributes $\leqslant 1\%$.

		Energy (MeV)		Wave function			
J_i^π	T	Expt.	Theor.	%	Partition	N_1	N_2
$7/2_1^-$	1/2	1.611	1.192	49	[12,4,4,1,0,0,0]	10	5
				14	[10,6,4,1,0,0,0]		
				12	[12,6,2,1,0,0,0]		
$9/2_1^-$	1/2	3.185	2.812	29	[12,4,4,1,0,0,0]	10	5
				24	[12,5,3,1,0,0,0]		
				12	[11,6,3,1,0,0,0]		
$11/2_1^-$	1/2	3.706	3.498	46	[12,4,4,1,0,0,0]	10	5
				12	[12,5,3,1,0,0,0]		
$9/2_2^-$	1/2	4.022	4.698	57	[12,4,4,1,0,0,0]	12	5
				11	[12,5,3,1,0,0,0]		
$9/2_3^-$	1/2	4.872	5.339	40	[12,4,4,1,0,0,0]	12	6
				19	[12,5,3,1,0,0,0]		
				12	[11,5,4,1,0,0,0]		
$11/2_2^-$	1/2	4.887	4.716	55	[12,4,4,1,0,0,0]	10	4
				16	[12,5,3,1,0,0,0]		
$11/2_3^-$	1/2	5.618	5.749	40	[12,4,4,1,0,0,0]	12	8
				19	[12,5,3,1,0,0,0]		
$13/2_1^-$	1/2	5.793	5.608	32	[11,5,4,1,0,0,0]	9	4
				19	[12,5,3,1,0,0,0]		
				11	[12,4,4,1,0,0,0]		
				10	[12,6,2,1,0,0,0]		
$13/2_2^-$	1/2	6.397	6.376	73	[12,4,4,1,0,0,0]	7	4
$15/2_1^-$	1/2	7.013	6.832	28	[11,5,4,1,0,0,0]	9	4
				22	[12,4,4,1,0,0,0]		
				19	[12,5,3,1,0,0,0]		

structure (i.e., $m_1, m_2, \ldots, m_n$) of different partitions having $> 10\%$ contribution are shown in the tables (Tables III and IV). The partitions are given in terms of occupation numbers of single-particle valence states. Here, N_1 is the total number of particle partitions for a particular state, each with contribution $>1\%$, and N_2 gives an estimation of the minimum number of particle partitions, each of which contributes $\leqslant 1\%$ in the state.

Tables III and IV show that the two low-lying positive parity states ($3/2^+$ and $7/2^+$) have basically multiplet structure. They have a much smaller extent of configuration mixing with the largest contribution $\approx$83% from a single partition. However, the configuration mixing in terms of particle partitions for the high spin positive parity states ($9/2^+$–$21/2^+$) has been increased. It was found that they have 10–17 particle partitions contributing at least 1% with the largest 19–49% particle partitions in their wave functions. For the negative parity yrast states, 28–49% particle partitions with 9–10 particle partitions contributing at least 1% in their wave functions were found. For the non-yrast negative parity states except $13/2_2^-$, 40–57% particle partitions with 10–12 particle partitions contributing at least 1% in their wave functions were found. Therefore, these negative parity states and high spin positive parity states show substantial configuration mixing in terms of particle partitions, which give us an indication of the presence of collective excitations at higher excitation energy in ^{37}Ar. The reduced transition probabilities [$B(E1)$, $B(M1)$, $B(E2)$, and $B(M2)$] for a few transitions were calculated by using the effective charges $e_p = 1.5$e and $e_n = 0.5$e and free values of g factors. The experimental transition strengths are calculated from the reported level lifetimes [1]. The branching and mixing ratios are taken from the present measurement. Most of the calculated values show good agreement with the corresponding experimental data (Table V), which provide evidence in favor of the reliability of the calculated wave functions. Calculated strengths for the decay out transitions from 4022-keV ($9/2_2^-$), 5214-keV ($11/2_1^+$), and 6151-keV ($13/2^+$) levels deviated to a large extent from the experimental values. This is might be an indication of the fact that the wave functions for these states are not well reproduced in the calculation. We also calculated the branching ratios for a few levels and compared them with the experimental branching ratios (Table II).

The energy spectra for γ transitions from 5618-, 6397-, 7013-, 9091-, 9881-, and 10574-keV levels in ^{37}Ar were fully shifted (Fig. 5). None of them have any stopped component. These γ's are therefore emitted in flight and the lifetime of these levels must be shorter than the stopping time of the

TABLE V. Comparison of experimental and theoretical reduced transition probabilities for different transitions in ^{37}Ar.

E_x	τ_{mean} (ps)	E_γ	$B(E1)$ ($\times10^{-6}$ e^2fm^2)		$B(M1)$ ($\times10^{-3}\mu_N^2$)		$B(E2)$ (e^2fm^4)		$B(M2)$ (μ_N^2fm^2)	
(keV)	Reported [1]	(keV)	Expt.	Theor.	Expt.	Theor.	Expt.	Theor.	Expt.	Theor.
1611	6.3(2)[a]	1611							1.04(6)	2.05
2217	0.41(3)	2217					36.5(34)	41.3		
3185	0.28(1)	1574			42(3)	36				
3706	0.37(2)	521			160(10)	197				
		2095					45(3)	41		
4022	0.04(1)	837			420(150)	84				
		1805	2000(700)	1078						
		2411			6.2(22)	3.46				
5214	3.7(4)	1192	10.3(15)	110.3						
		1508	19(2)	51.27						
		2029	3.8(4)	109						
		3603							1.8(4)	3.9
5793	0.05(1)	906			47(13)	59				
		2087			48(14)	13				
		2608					77(21)	55		
6151	4.5(4)	937			11.1(11)	4.9				
		1264	12.4(14)	5.9						
		2445	0.28(3)	317						
6474	7.1(10)	323			100(20)	103				
		681	70(10)	14.8						
		1260					9.3(14)	10.2		
		2768							1.4(2)	1.6
7072	0.54(12)	598			480(100)	498				

[a]In ns.

recoils (^{37}Ar) in Au backing. We calculated the stopping time [33] of ^{37}Ar in the Au backing using the calculated range and the stopping power of ^{37}Ar in the Au backing [34]. The energy distribution of the recoils (^{37}Ar) is taken from PACE4 calculation [19]. The estimated stopping time of ^{37}Ar in the Au backing is $\approx$430 fs. So, the lifetimes of these levels must be shorter than 430 fs. In the present work, we did not perform lifetime measurement to extract their lifetimes. But we calculated their lifetimes from shell model calculations. We first calculated the transition strengths of the decay out 1912-, 2019-, 3307-, and 3502-keV transitions and then extracted the level lifetimes from their calculated transition strengths, branchings, and mixing ratios. Since the spins and parities of 6397- and 9881-keV levels are not confirmed, we did not calculate their lifetimes. The calculated lifetimes of 5618-, 7013-, 9091-, and 10574-keV levels are shown in Table VI. The results obtained from shell model calculations agree well with our experimental observations. However, the calculated multipole mixing ratio (δ) of 2019-keV transition ($\delta = 1.72$) does not agree with the experimental value $\delta = 0.01(5)$.

D. Two-level mixing calculation

In case of positive parity states, we have seen that the calculated unperturbed energies of the yrast $9/2^+$, $11/2^+$ and $13/2^+$ states generated from 0p-0h excitation are 8326-, 7497-, and 14289-keV, respectively. On the other hand, the calculated unperturbed energies of the yrast $9/2^+$, $11/2^+$, and $13/2^+$ states generated from 2p-2h excitation are 5911-, 5825-, and 6545-keV, respectively. The latter energies are close to the experimental energies. So one may expect an admixture of 0p-0h configuration into the 2p-2h configuration for these states. Hence, a phenomenological approach following the discussion as in Ref. [35], using two-level mixing between pure 2p-2h and 0p-0h states, was used to determine the extent of configuration mixing in $9/2^+$, $11/2^+$, and $13/2^+$ states. In this calculation, $9/2^+$, $11/2^+$, and $13/2^+$ states were assumed to be dominated by the 2p-2h configuration with

TABLE VI. Calculated lifetimes of 5618-, 7013-, 9091-, and 10574-keV levels in ^{37}Ar.

E_x	E_γ			$B(M1)$ ($\times10^{-3}\mu_N^2$)	$B(E2)$ (e^2fm^4)	Branching (%)	δ	τ_{mean} (fs)
(keV)	(keV)	J_i	J_f	Theor.	Theor.	Theor.	Theor.	Theor.
5618	1912	$11/2^-_3$	$11/2^-_1$	93.2	1.3	99	0.06	84.8
7013	3307	$15/2^-_1$	$11/2^-_1$		66.6	100	0	30.3
9091	2019	$19/2^+$	$17/2^+$	8.19	85.4	100	1.72	209.9
10574	3502	$21/2^+$	$17/2^+$		16.4	100	0	56.6

TABLE VII. Amount of 0p-0h configuration mixing in $9/2^+$, $11/2^+$, and $13/2^+$ states obtained from two-level mixing calculation. All energies are in keV.

	Energy		Mixing	Energy	
J_i^π	2p-2h	0p-0h	(%)	Mixed	Expt.
$9/2^+$	5911	8326	14	5444	5437
$11/2_1^+$	5825	7497	21	5217	5214
$11/2_2^+$	6555	16376	4.8	6034	6031
$13/2^+$	6545	14289	4.5	6209	6151

a small amount of 0p-0h configuration mixing. Utilizing the unperturbed energies of yrast $9/2^+$, $11/2^+$, and $13/2^+$ states obtained from pure 0p-0h and 2p-2h calculations, the experimental energies of these states were reproduced considering the mixing coefficient of the 0p-0h configuration for each state as a variable. The results of the two-level mixing calculation are shown in Table VII. It shows that 14%, 21%, and 4.5% of 0p-0h configuration mixing reproduces the experimental energies of the yrast $9/2^+$, $11/2^+$, and $13/2^+$ levels, respectively. The estimated 0p-0h mixing in the $11/2_2^+$ level is 4.8%. In the neighboring isotopes of ^{37}Ar, the high spin positive parity states generated from 4p-4h excitation appear at relatively lower excitation energies [2,10]. The excitation energies of the bandhead 2^+ state generated from 4p-4h excitation in ^{36}Ar and ^{38}Ar are 4951 and 4566 keV, respectively. In ^{37}Ar, one may therefore expect positive parity states generated from 4p-4h excitation in this energy domain. As a result, the observed positive parity states ($9/2^+$, $11/2^+$, and $13/2^+$) may also have mixing from 4p-4h configuration. Since, the full space calculation is not possible for 4p-4h excitation, we could not extract the amount of 4p-4h configuration mixing for these states. It should be noted that the mixing of configurations from different np-nh ($n\hbar\omega$, $n = 0, 2, 4, 6, 8$) excitations on a particular positive parity excited state have already been reported in the neighboring ^{36}Ar, ^{38}Ar, and ^{40}Ca nuclei [5,36].

The observed negative parity states in ^{37}Ar are primarily generated from 1p-1h excitation. But the calculated energies for all the negative parity states, obtained from the 1p-1h excitation calculation, are underpredicted as discussed above. The calculated energies obtained from 3p-3h excitation are higher than the energies obtained from 1p-1h excitation. So, if we consider configuration mixing between 1p-1h and 3p-3h excitations, it will further push down the energies of the mixed states dominated by 1p-1h configuration and increase their deviation from the experimental energies. So, we have not performed the mixing calculation for the negative parity states.

V. CONCLUSION

High spin states of ^{37}Ar populated through the ^{27}Al(^{12}C, np)^{37}Ar reaction with a 40 MeV ^{12}C beam, were studied using the Indian National Gamma Array (INGA) facility. The existing level scheme has been extended up to 10.5 MeV by adding 8 new levels and 18 new transitions. The spins and parities of most of the levels have been assigned, modified, or confirmed from $R_{\rm DCO}$ and linear polarization measurements. For a few weak transitions, $R_{\rm ADO}$ measurements were carried out to assign their dipole or quadrupole nature. The multipole mixing ratios (δ) for most of the transitions were measured and compared with the earlier measurements wherever available. We have identified a few levels at higher excitation energy whose level lifetimes are expected to be smaller than 430 fs. Large basis shell model calculations were performed to understand the microscopic origin of these levels. In our calculations, different particle restrictions in *sd* and *pf* orbitals were used to reproduce the experimental level scheme. A simple two-level mixing calculation was also performed to extract the amount of 0p-0h and 2p-2h configuration mixing for yrast $9/2^+$, $11/2^+$, and $13/2^+$ levels. The improvement of calculated energies shows a necessity for multiparticle multihole configuration mixing of a few levels. Only two low-lying states in ^{37}Ar, viz., $3/2^+$ and $7/2^+$, are of single-particle nature. Beyond that, both positive and negative parity states exhibit tendency towards collectivity as manifested by their wave functions. The experimental transition strengths for most of the transitions were compared with the calculated values. The lifetimes of four new levels were also calculated and compared with the experimental observations.

ACKNOWLEDGMENTS

The authors sincerely thank P. K. Das (SINP), S. K. Jadhav (TIFR), and P. B. Chavan (TIFR) for their technical help before and during the experiment. Thanks are due to the target laboratory of VECC, Kolkata for preparation of the target. Special thanks are due to the Pelletron staff for a nearly uninterrupted beam. This work has been partially funded by the Department of Science and Technology, Government of India (Grant No. IR/S2/PF-03/2003-II).

[1] http://www.nndc.bnl.gov
[2] C. E. Svensson *et al.*, Phys. Rev. Lett. **85**, 2693 (2000); Phys. Rev. C **63**, 061301(R) (2001).
[3] E. Ideguchi *et al.*, Phys. Rev. Lett. **87**, 222501 (2001); C. J. Chiara, E. Ideguchi, M. Devlin, D. R. LaFosse, F. Lerma, W. Reviol, S. K. Ryu, D. G. Sarantites, C. Baktash, A. Galindo-Uribarri, M. P. Carpenter, R. V. F. Janssens, T. Lauritsen, C. J. Lister, P. Reiter, D. Seweryniak, P. Fallon, A. Gorgen, A. O. Macchiavelli, and D. Rudolph, Phys. Rev. C **67**, 041303(R) (2003).
[4] A. Bisoi *et al.*, Phys. Rev. C **88**, 034303 (2013).
[5] E. Caurier, F. Nowacki, and A. Poves, Phys. Rev. Lett. **95**, 042502 (2005); E. Caurier, J. Menèndez, F. Nowacki, and A. Poves, Phys. Rev. C **75**, 054317 (2007).
[6] T. Sakuda and S. Ohkubo, Phys. Rev. C **49**, 149 (1994).
[7] T. Sakuda and S. Ohkubo, Nucl. Phys. A **744**, 77 (2004); **748**, 699 (2005).
[8] A. Bisoi *et al.*, Phys. Rev. C **97**, 044317 (2018).
[9] A. Bisoi *et al.*, Phys. Rev. C **90**, 024328 (2014).
[10] D. Rudolph *et al.*, Phys. Rev. C **65**, 034305 (2002).

[11] E. Ideguchi *et al.*, Phys. Lett. B **686**, 18 (2010).
[12] S. Ray *et al.*, Proc. DAE-BRNS Symp. Nucl. Phys. (India) **53**, 353 (2008).
[13] J. Cameron *et al.*, Nucl. Data Sheets **113**, 365 (2012).
[14] E. K. Warburton *et al.*, Phys. Rev. C **14**, 996 (1976).
[15] R. Palit *et al.*, Nucl. Instrum. Methods A **680**, 90 (2012).
[16] H. Tan *et al.*, in *Nuclear Science Symposium Conference Record 2008* (IEEE, Washington, 2008), p. 3196.
[17] R. K. Bhowmik *et al.*, Proc. DAE-BRNS Symp. Nucl. Phys. (India) B **44**, 422 (2001).
[18] D. C. Radford, Nucl. Instrum. Methods A **361**, 297 (1995).
[19] A. Gavron, Phys. Rev. C **21**, 230 (1980).
[20] E. S. Macias, W. D. Ruthter, D. C. Camp, and R. G. Lanier, Comput. Phys. Commun. **11**, 75 (1976).
[21] A. Bisoi, Investigation of interplay of single particle and collective excitation in atomic nuclei, Ph.D. thesis, University of Calcutta, 2014, https://shodhganga.inflibnet.ac.in/handle/10603/163753.
[22] K. Starosta *et al.*, Nucl. Instrum. Methods A **423**, 16 (1999).
[23] E. D. Mateosian *et al.*, At. Data Nucl. Data Tables **13**, 391 (1974).
[24] A. Bisoi *et al.*, Phys. Rev. C **89**, 024303 (2014).
[25] M. Saha Sarkar, in *The 8th International Conference on Progress in Theoretical Physics (ICPTP 2011), 23–25 October 2011, Constantine, Algeria*, edited by N. Mebarki, J. Mimouni, N. Belaloui, and K. Ait Moussa, AIP Conf. Proc. No. 1444 (AIP, New York, 2012), p. 188; M. Saha Sarkar *et al.*, in *Frontiers in Gamma-Ray Spectroscopy 2012 - FIG12, 5–7 March 2012, New Delhi, India*, edited by S. Muralithar, AIP Conf. Proc. No. 1609 (AIP, New York, 2014), p. 95.
[26] A. Das *et al.*, Proc. DAE-BRNS Symp. Nucl. Phys. (India) **62**, 82 (2017), http://www.sympnp.org/proceedings/index.php.
[27] L. L. Gadeken *et al.*, J. Phys. A (London) **7**, 83 (1974); P. J. Nolan *et al.*, J. Phys. G (London) **1**, 35 (1975).
[28] H. J. Rose and D. M. Brink, Rev. Mod. Phys. **39**, 306 (1967).
[29] K. S. Krane and R. M. Steffen, Phys. Rev. C **2**, 724 (1970).
[30] B. A. Brown *et al.*, MSU-NSCL Report No. 1289, 2004 (unpublished).
[31] E. K. Warburton, J. A. Becker, and B. A. Brown, Phys. Rev. C **41**, 1147 (1990).
[32] R. Kshetri *et al.*, Nucl. Phys. A **781**, 277 (2007)
[33] G. F. Knoll, *Radiation Detection and Measurement*, (John Wiley and Sons, New York, 1979).
[34] J. F. Ziegler, J. Biersack, and U. Littmark, *The Stopping and Range of Ions in Matter* (Pergamon, Oxford, 1985), http://www.srim.org
[35] P. J. Brussard and P. W. M. Glaudemans, *Shell-Model Applications in Nuclear Spectroscopy* (North-Holland, Amsterdam, 1977); R. F. Casten, *Nuclear Structure from a Simple Perspective* (Oxford University Press, New York, 1990).
[36] S. Courtin *et al.*, J. Phys.: Conf. Ser. **436**, 012051 (2013); A. F. Lisetskiy *et al.*, Nucl. Phys. A **789**, 114 (2007).